Groove-structured meta-surface for patterned sub-diffraction sound focusing

Chen, Jian; Sun, Zeqing; Fan, Zheng

2019

Chen, J., Sun, Z., & Fan, Z. (2019). Groove-structured meta-surface for patterned sub-diffraction sound focusing. Applied Physics Letters, 114(25), 254102-. doi:10.1063/1.5096258

https://hdl.handle.net/10356/106321

https://doi.org/10.1063/1.5096258

Applied Physics Letters ARTICLE scitation.org/journal/apl

Groove-structured meta-surface for patterned sub-diffraction sound focusing

Cite as: Appl. Phys. Lett. **114**, 254102 (2019); doi: 10.1063/1.5096258
Submitted: 15 March 2019 · Accepted: 9 June 2019 ·
Published Online: 25 June 2019

Jian Chen, Zeqing Sun, and Zheng Fan[a)]

AFFILIATIONS

School of Mechanical and Aerospace Engineering, Nanyang Technological University, 50 Nanyang Avenue, Singapore 639798

[a)]Author to whom correspondence should be addressed: ZFAN@ntu.edu.sg

ABSTRACT

Confining acoustic fields in subwavelength volumes is of fundamental interest in wave-energy harvesting and high-resolution imaging. Phononic crystals have been shown to be capable of superfocusing but are highly limited by their very large dimensions. Acoustic metasurfaces can yield similar functionality with unit cells significantly smaller than the wavelength. However, they are studied mostly under effective medium theory and cannot manipulate evanescent waves directly to control near-field focusing. Here, we use a microscopic approach to study acoustic metasurfaces for subdiffraction focusing of reflected waves, which consist of an array of deep-subwavelength sized and spaced grooves. We further show that the focusing pattern can be tailored by the designer. To validate the effectiveness of our scheme, two representative metasurfaces are designed theoretically, proved numerically, and confirmed experimentally for subdiffraction sound focusing with different patterns. We hope that our approach can work as a general guideline to shape near-field signals in the broad field of acoustics.

Confining acoustic waves in subwavelength volumes to enhance the acoustic fields is of fundamental interest in wave physics and highly desirable for various applications in acoustics, such as high-resolution imaging, high-intensity focused ultrasound treatment, enhanced sensing, highly efficient wave-energy harvesting, and so on. Conventionally, acoustic focusing is limited by diffraction, which can be characterized by the Rayleigh criterion, $B = 0.61\ \lambda/NA$, where λ is the incident acoustic wavelength and NA represents the numerical aperture of focusing elements.[1] Such limitations arise from the quick fading of evanescent waves because of their exponential decaying nature upon propagation. To break the diffraction limit, evanescent waves bound in the near field should be involved and contribute to the formation of the target focus.[2–4]

In the last few decades, substantial efforts have been made on this subject, which can be traced back to Pendry's perfect lens, showing that a subwavelength source can be restored by recovering evanescent fields through a negative-index slab.[5] Since then, negative refraction has been studied extensively and various negative-index devices to manipulate acoustic waves have been developed.[6–13] Phononic crystals were first investigated and theoretically and experimentally demonstrated for superfocusing by Bragg scattering at the Brillouin zone.[8,9,11] However, because of the wavelength-scale lattice periodicity, the phononic crystals are generally extremely huge in size, which hampers their widespread use in practice. By contrast, acoustic metamaterials have alleviated the dimensional concerns by engineering the unit cells on spatial scales considerably smaller than the wavelength. With appropriate arrangement, acoustic metamaterials with unprecedented functionalities, such as large refractive indices,[14,15] negative effective density,[16,17] bulk modulus,[18] or both,[19,20] have been demonstrated. Moreover, they have stimulated numerous applications, including sound focusing.[12,21–23] Because of the subwavelength nature of the unit cells, acoustic metamaterials are commonly studied under effective medium theory to consider their macroscopic properties and predict the behavior of evanescent waves. Although great success has been achieved using the aforementioned methods, direct control of the acoustic near field to create a subdiffraction focus remains largely unexplored, making the task of determining an optimum structure with good performance difficult.

Very recently, we have demonstrated subdiffraction focusing of acoustic waves with a metasurface consisting of an array of deep-subwavelength sized and spaced slits.[24] By exploiting full-wave dynamics on the metasurface, the acoustic evanescent waves in the near field can be manipulated directly. However, the previous development was demonstrated primarily in the transmission mode, whereby achieving high field enhancement is difficult because most acoustic energies are reflected. Moreover, only a fraction of the evanescent wave components can pass through the metasurface because of its bandpass effect. Nevertheless, such deficiency can be turned into an asset if a metasurface can be crafted to manipulate the reflected waves.

The current study proposes a near-field metasurface for subdiffraction sound focusing in the reflection mode, which is composed of a thin plate imperforated with an array of grooves that are deep-subwavelength in size and spacing [Fig. 1(a)]. The grooves are set up to excite the acoustic evanescent waves and modulated to form a prescribed focus in the near field by tuning their geometry, that is, the width, properly. To understand the underlying physics and provide a comprehensive rule for the near-field metasurface design, we extend our previous model to describe the behavior of scattering waves as well as their interaction in the groove structures. Based on the microscopic model, acoustic evanescent waves can be manipulated directly to produce desired focusing action. For proof-of-concepts, two examples of the near-field metasurfaces are optimized for subdiffraction focusing based on the design rule. The focusing performance is investigated further through numerical simulations and experimental characterization studies to demonstrate the effectiveness of the proposed scheme. Beyond the subdiffraction focusing, our concept is anticipated to be applicable as a general guideline to mold near-field signals in various scenarios.

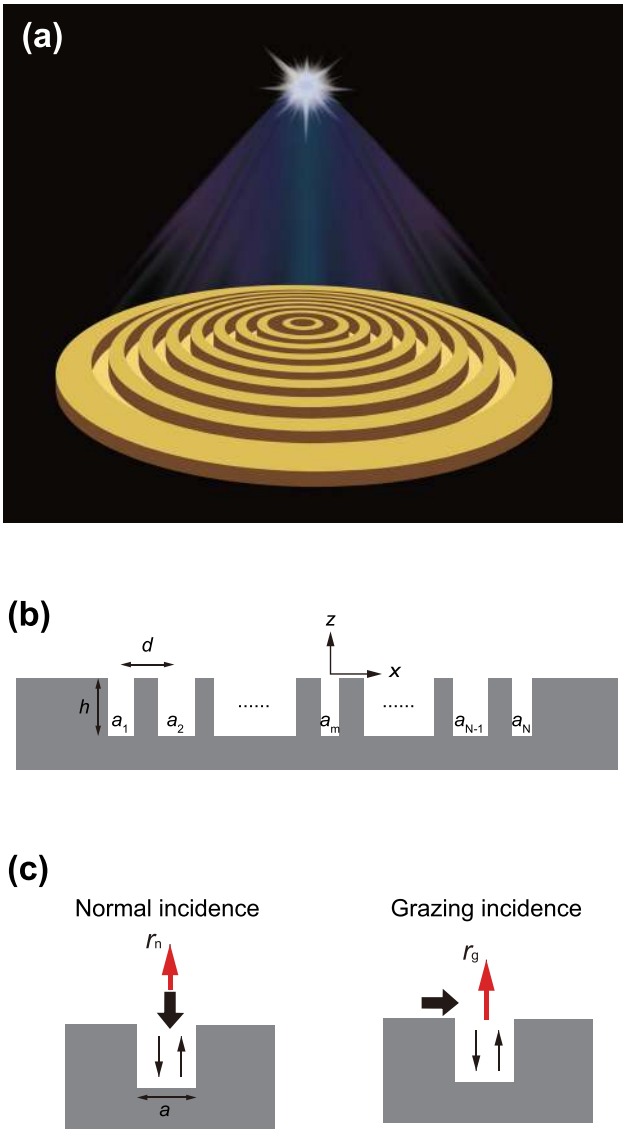

FIG. 1. (a) Schematic of the near-field metasurface for subdiffraction sound focusing. (b) Schematic of the cross section of the groove-structured metasurface. It consists of N grooves that are imperforated in a thin plate with a spacing of d and a depth of h. The plate thickness and groove width are denoted by H and a_m, respectively. (c) The reflection coefficients of a subwavelength groove under normal (left) and grazing (right) incidences.

Figure 1(b) illustrates schematically the cross section of the near-field metasurface. It consists of N grooves with a period of d and a depth of h. The widths of the grooves are denoted by a_m, where m $= 1,\ldots,N$. The thickness of the plate is H. From a microscopic view, the grooves can be considered a set of modulated, aperiodic emitters. The focusing action is governed by the waves launched by individual emitters. The normally incident wave is first scattered by the grooves, and the scattered wave can be regarded as a new emission source. When created, the emitting waves will propagate along the surface and interact with other grooves. Apparently, wave scattering from a single groove under normal and grazing incidences is the basis for calculating the entire scattering field. Hence, we begin with the fundamental process of wave interaction with a subwavelength groove, which can be described by employing the mode expansion method[25,26] as depicted in Fig. 1(c). The reflection coefficients for normal and grazing incidences are defined as r_n and r_g, respectively. According to the boundary condition, the zero-order cavity mode of the pressure and velocity fields inside the groove should match those of the plane wave expansions outside the groove at the interface (i.e., $z = 0$). Consequently, the coefficient can be expressed as $r_n = \frac{2(1+e^{2ik_0h})}{(1+Q)+(1-Q)e^{2ik_0h}} - 1$ and $r_g = \frac{(1+e^{2ik_0h})\mathrm{sinc}\left(\frac{k_0a}{2}\right)}{(1+Q)+(1-Q)e^{2ik_0h}} - 1$, respectively; $k_0 = 2\pi/\lambda$ is the wavenumber in free space, a denotes the groove width, and $Q = \frac{k_0}{\pi a}\int_{-\infty}^{\infty} \frac{1-\cos(a\eta)}{\eta^2\sqrt{k_0^2-\eta^2}}\,d\eta$, which accounts for the coupling of the fundamental cavity mode and all the diffractive waves for a subwavelength cavity (i.e., groove). At this point, the behavior of the scattering acoustic wave, or acoustic response, from a groove can be readily adjusted by tuning its geometry, width or depth or both.

Other than the reflection coefficient, another important aspect of the acoustic response is its propagation. Although calculating the field distribution analytically is viable through the acoustic wave equation and mode analysis, we use a numerical study instead for convenience to characterize the propagation. For a diffractive subwavelength source of unity amplitude, its pressure field distribution can be expressed as $p(s) = \beta e^{i\phi} H_0^{(2)}(k_0 s)$,[27] where β and ϕ are the characteristic parameters of the propagation function, s is the distance from the source, and $H_0^{(2)}$ is the zeroth-order Hankel function of the second kind. Similarly, a semianalytical two-step method is adopted to determine β and ϕ (see Ref. 24 for further details). For this step, we can generate a large database for these two parameters by sweeping the possible groove geometries that can serve as a design library. For simplicity, we extract β and ϕ for a number of groove widths (40 here) and fit them to a four-order polynomial function using the least-mean squares method as shown in Fig. 2. The fitted polynomials are $\beta(u = a/\lambda) = -603.4u^4 + 312u^3 - 59.9u^2 + 6.53u + 0.274$ and $\phi(u = a/\lambda) = -549.1u^4 + 280.9u^3 - 53.89u^2 + 6.4u - 1.284$, respectively, with a determination coefficient $R^2 > 0.99$.

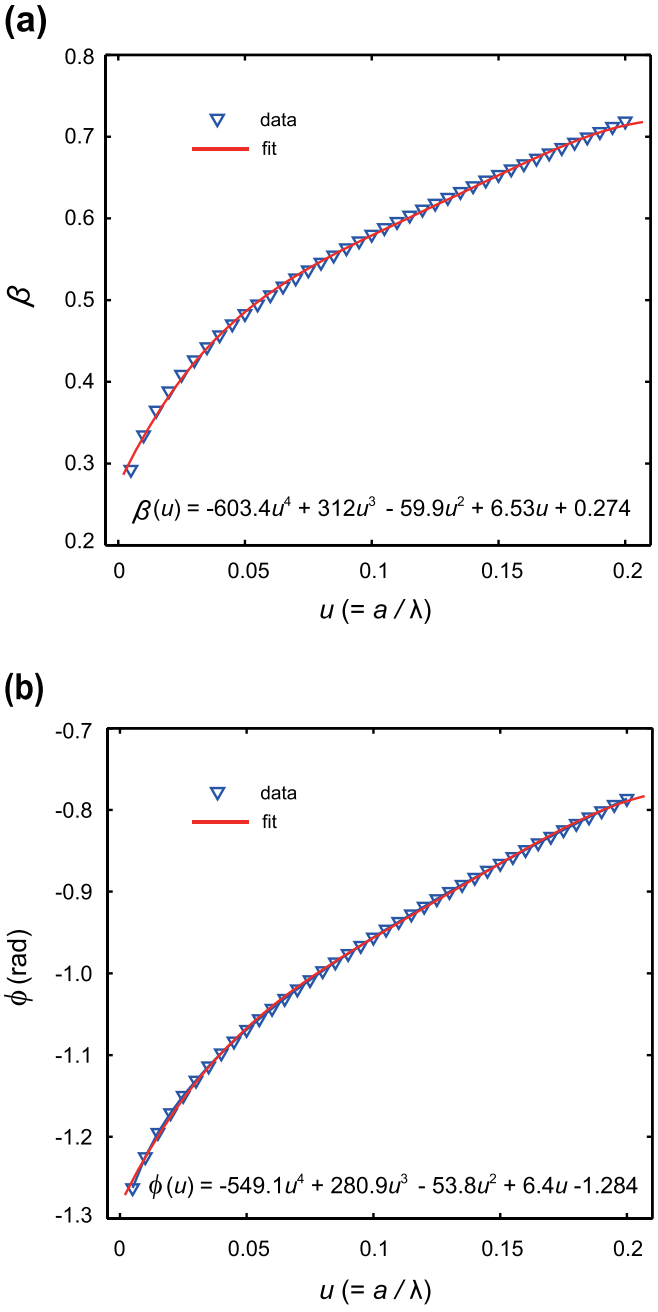

FIG. 2. The dependency of (a) β and (b) ϕ on the groove width. A 4-order polynomial curve is fitted to the data by the least-mean squares method.

Given that the acoustic response of the unit cell is acknowledged, we extended our previously developed microscopic coupled-wave model to the groove structures. Based on this model, manipulating acoustic evanescent waves directly becomes possible. Conversely, it can be utilized to optimize the metasurface for subdiffraction focusing through nonlinear least squares inversion, which fits the calculated field required to produce a focusing image. To corroborate this proposition, we first consider an acoustic metasurface for subdiffraction focusing of reflected waves, with a focal length of $L = 0.3\lambda$ and a field pattern of $p(x, z = L) = Ae^{-\frac{1}{4\ln 2}\left(\frac{x}{\mathrm{FWHM}}\right)^2} + p_0$ at the focal plane, where A is the amplitude, FWHM represents the full width at half maximum, and p_0 is the plane wave reflection. For convenience, we demonstrate the sound focusing in air with unity-amplitude plane wave incidence. Under such a circumstance, a mirror reflection occurs due to the very large impedance mismatch, and therefore, p_0 is determined to be 1 Pa. Also, the dimensional quantities are scaled to the wavelength in this context, with which the metasurface can be implemented at any frequency. For a particular design, the focal pattern was set as $A = 1$ and FWHM $= 0.35\lambda$. Generally, the metasurface aperture, that is, $(N - 1)\ d$, is determined by the focal length and spot size: the longer the focal length, the bigger the spot and the larger the aperture. On the other hand, the groove depth has a remarkable influence on the spatial-frequency spectrum of the excited evanescent waves. A higher spatial-frequency evanescent wave can be generated with a deeper groove, and vice versa, in the range of $[0, 0.25\lambda]$. As a result, the preset geometrical parameters are set to $h = \lambda/6$, $d = 0.15\lambda$, and $N = 11$. According to studies on microwaves,[28,29] the field in the working region $(z > 0)$ can be determined uniquely from the boundary values. Thus, we use the acoustic field at the surface, that is, the aperture field located at $z = 0$, for the optimization. Accordingly, the aperture field was derived through back propagation.[28] We optimized the metasurface by using the nonlinear least squares solver in Matlab 2013b based on the aperture field, and the resulting groove widths are listed in Table I.

To study the performance of the optimized metasurface (AMS 1) in subdiffraction focusing, we first modeled it using the finite element method (FEM) software COMSOL Multiphysics 5.1. In the FEM simulation, pressure acoustics and solid mechanics modules are incorporated. A plane wave is normally incident on the groove-structured metasurface. Figure 3(b) shows the normalized intensity distribution of the reflected pressure field from the simulation. As expected, a focal spot is clearly formed in the front of the metasurface. For comparison, we also plotted in Fig. 3(a) the intensity of the calculated pressure field using the microscopic model. Apparently, the two maps are in good agreement with each other, which primarily demonstrates the effectiveness of our scheme. To confirm the focusing behavior experimentally, we fabricated the sample metasurface at the wavelength of $\lambda = 300$ mm using wire cutting. The acoustic field was recorded using a field mapping technique.[24] The field reflected from the metasurface was obtained by scanning the reflected region without the metasurface and the field with the metasurface and then calculating the difference between these two fields. The measured result is shown in Fig. 3(c), which coincides well with the calculated and simulated images. For a quantitative analysis, Fig. 3(d) illustrates the amplitude profiles of the reflected pressure field at the focal plane [white dashed line in

TABLE I. Optimized groove widths of AMS 1.

Groove	1	2	3	4	5	6
Width	0.005λ	0.005λ	0.006λ	0.103λ	0.1λ	0.017λ
Groove	7	8	9	10	11	
Width	0.1λ	0.103λ	0.006λ	0.005λ	0.005λ	

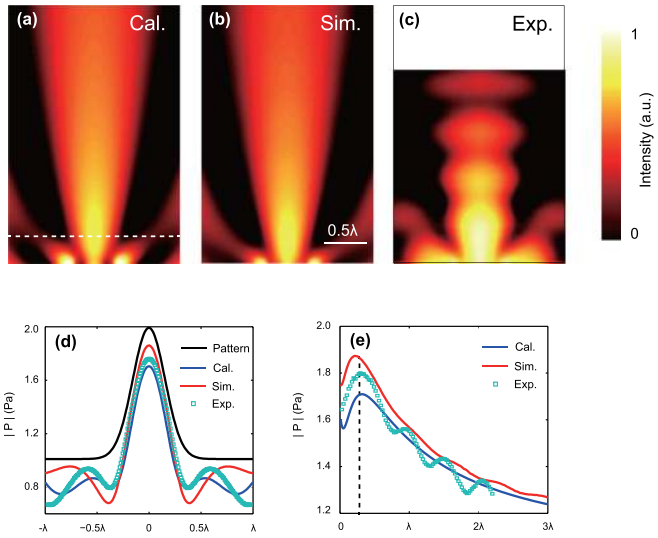

FIG. 3. The normalized intensity distribution of (a) calculated, (b) simulated, and (c) measured pressure fields reflected from AMS 1. The white dashed line denotes the designated focal plane. The amplitude profiles of the pressure field through the focal spot along (d) transverse and (e) axial directions.

Fig. 3(a)]. As a reference, the predesigned focal pattern is also plotted, which coincides well with the calculation, simulation, and experiment, showing that subdiffraction sound focusing is effectively achieved. Moreover, the calculated, simulated, and measured FWHMs are found to be 0.37λ, 0.38λ, and 0.39λ, respectively, all of which are close to the designation of 0.35λ. As the peak amplitude, the calculated, numerical, and measured results are 1.71, 1.86, and 1.78 slightly lower than the theoretical value, respectively. Furthermore, Fig. 3(e) shows the profiles of the pressure amplitude along the axial direction, from which the calculated, simulated, and measured focal lengths are measured to be 0.31λ, 0.28λ, and 0.3λ, respectively. These good agreements prove the accurate control of acoustic waves in the near field. Alternately, the slight discrepancies in the FWHM, focal length, and amplitude are mainly attributed to the discretion effect of the aperture field in the optimization. Moreover, as the grooves were simplified as simple point sources in the calculation, the calculated peak amplitude is slightly smaller than both simulation and experiment, considering that a wider groove typically makes more contribution to the focusing. It is also worth noting that a broadband focusing may be expected for the groove-structured metasurface. This is because the wave dynamics mainly come from the diffractions and couplings between these deep-subwavelength structures. For this reason, the focusing behavior is robust even when the input frequency changes, as long as the metasurface operates on the deep-subwavelength scale.[30]

To illustrate the generality of the proposed method, we illustrate another metasurface (AMS 2) based on the same procedure. In this demonstration, the focal length and focal pattern are set to $L = 0.1\lambda$ and $p(x, z = L) = A\mathrm{sinc}(qx) + p_0$, respectively, with $A = 2$ and $q = 3.0\ k_0$ being the cutoff wavenumber, which yields a FWHM of 0.17λ. For the preset parameters, we change the groove depth and spacing to 0.19λ and 0.1λ, respectively; by contrast, the groove number remains the same, that is, $N = 11$. Similarly, the aperture field is first back propagated, with which the metasurface is then optimized. The optimized results are provided in Table II. Similarly, numerical simulation and experimental measurements were conducted to check the focusing performance. Figures 4(a)–4(c) show the normalized intensity patterns of the calculated, simulated, and measured pressure fields reflected from AMS 2. Convincingly, a tight subdiffraction focus near the metasurface can be observed in all images, readily proving the capability of subdiffraction focusing. However, unlike the previous design, these figures show a behavior reminiscent of beam coupling that the beam diffraction of a particular source is prevented by the presence of its neighbors. The central beam spreads out after the intensity of its neighbors weakened to a certain amount, and the focal length is determined by the point at which this phenomenon occurs (white dashed line).[29] Therefore, the focal length is found to be 0.11λ, which is consistent with the design. Then, the pressure amplitude profiles at the focal plane are plotted in Fig. 4(d), which are 2.68, 2.77, and 2.72, respectively, for the calculation, simulation, and measurement. For what concerns the FWHM, the calculated, simulated, and measured results are 0.18λ, 0.19λ, and 0.21λ, respectively, all of which coincide with the expected value. These findings once again confirm the effectiveness of the proposed scheme. The same as above, the slight enlargement of the focal spot and reduction in the amplitude come from the discretization effect in the optimization process and can be accomplished readily using numerical simulations.

TABLE II. Optimized groove widths of AMS 2.

Groove	1	2	3	4	5	6
Width	0.017λ	0.023λ	0.01λ	0.114λ	0.004λ	0.056λ
Groove	7	8	9	10	11	
Width	0.004λ	0.114λ	0.01λ	0.023λ	0.017λ	

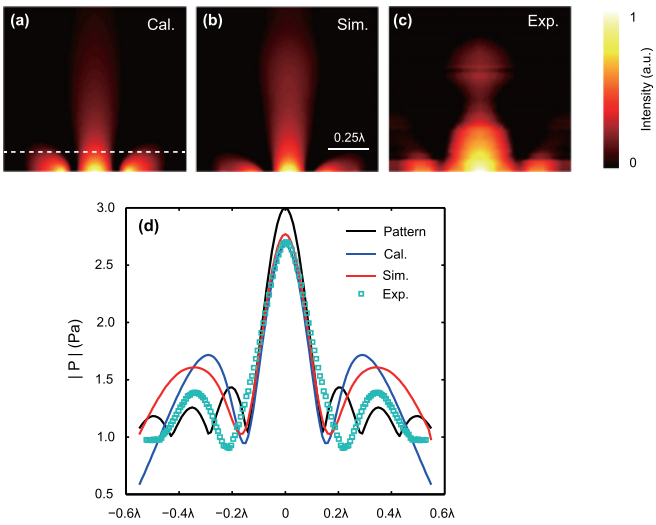

FIG. 4. The normalized intensity distribution of (a) calculated, (b) simulated, and (c) measured pressure fields reflected from AMS 2. The white dashed line denotes the focal plane. (d) The amplitude profiles of the pressure field at the focal plane.

In addition, several issues need to be addressed in the future, but beyond the scope of this work. First, the preset of geometrical parameters is critical for the inverse optimization, which may lead to local convergence with an improper assignment. Therefore, an in-depth investigation is necessary to draw up potential guidelines to facilitate the design process as well as the use of global optimization methods. Second, simultaneous control of the amplitude and phase for other forms of wave manipulation is also possible by tuning both the groove width and the depth under the same framework.

In summary, we present a microscopic approach to develop a groove-structured metasurface for subdiffraction sound focusing by directly manipulating the acoustic evanescent waves in the near field. Particularly, the focal pattern can be user-defined in various symmetries and shapes. A general design procedure is outlined for the design of such kinds of near-field devices. The first step is to determine the aperture field by back propagating a defined focal pattern. The second step involves optimizing the structural parameters to match the aperture field using the microscopic model. Following this procedure, two representative near-field metasurfaces are showcased theoretically, numerically, and experimentally to demonstrate the effectiveness of our scheme, all of which verify their capability to converge the reflected waves into a predesigned subdiffraction focus. Given that the near-field metasurfaces provide strong spatial confinement of acoustic fields with extreme simplicity, they hold promise for various potential applications, including but not limited to superresolution acoustic microscopy, near-field acoustic sensing, acoustic noise harvesting, and enhanced temperature elevation of therapeutic ultrasonic treatment.

This work was supported by the Ministry of Education Singapore under No. RG99/17.

REFERENCES

[1]J. W. Goodman, *Introduction to Fourier Optics*, 2nd ed. (McGraw-Hill, 1996).
[2]D. Lu and Z. Liu, Nat. Commun. **3**, 1205 (2012).
[3]R. Merlin, Science **317**, 927 (2007).
[4]J. H. Park, C. Park, H. Yu, J. Park, S. Han, J. Shin, S. H. Ko, K. T. Nam, Y. H. Cho, and Y. Park, Nat. Photonics **7**, 454–458 (2013).
[5]J. B. Pendry, Phys. Rev. Lett. **85**, 3966 (2000).
[6]X. Zhang and Z. Liu, Appl. Phys. Lett. **85**, 341 (2004).
[7]S. Yang, J. H. Page, Z. Liu, M. L. Cowan, C. T. Chan, and P. Sheng, Phys. Rev. Lett. **93**, 024301 (2004).
[8]Z. He, F. Cai, Y. Ding, and Z. Liu, Appl. Phys. Lett. **93**, 233503 (2008).
[9]A. Sukhovich, B. Merheb, K. Muralidharan, J. O. Vasseur, Y. Pennec, P. A. Deymier, and J. H. Page, Phys. Rev. Lett. **102**, 154301 (2009).
[10]V. Garcıa-Chocano, J. Christensen, and J. Sanchez-Dehesa, Phys. Rev. Lett. **112**, 144301 (2014).
[11]X. Zhou, M. Badreddine Assouar, and M. Oudich, Appl. Phys. Lett. **105**, 233506 (2014).
[12]N. Kaina, F. Lemoult, M. Fink, and G. Lerosey, Nature **525**, 77 (2015).
[13]J. H. Page, AIP Adv. **6**, 121606 (2016).
[14]Z. Liang and J. Li, Phys. Rev. Lett. **108**, 114301 (2012).
[15]Y. Li, G. Yu, B. Liang, X. Zou, G. Li, S. Cheng, and J. Cheng, Sci. Rep. **4**, 6830 (2014).
[16]S. H. Lee, C. M. Park, Y. M. Seo, Z. G. Wang, and C. K. Kim, Phys. Lett. A **373**(48), 4464 (2009).
[17]N. Sui, X. Yan, Y. Huang, J. Xu, F. Yuan, and Y. Jing, Appl. Phys. Lett. **106**, 171905 (2015).
[18]N. Fang, D. Xi, J. Xu, M. Ambati, W. Srituravanich, C. Sun, and X. Zhang, Nat. Mater. **5**, 452 (2006).
[19]S. H. Lee, C. M. Park, Y. M. Seo, Z. G. Wang, and C. K. Kim, Phys. Rev. Lett. **104**, 054301 (2010).
[20]T. Brunet, A. Merlin, B. Mascaro, K. Zimny, J. Leng, O. Poncelet, C. Aristégui, and O. Mondain-Monval, Nat. Mater. **14**, 384 (2015).
[21]S. Zhang, L. Yin, and N. Fang, Phys. Rev. Lett. **102**, 194301 (2009).
[22]X. Fan, Y. Zhu, B. Liang, J. Yang, and J. Cheng, Appl. Phys. Lett. **109**, 243501 (2016).
[23]Y. Zhu, J. Hu, X. Fan, J. Yang, B. Liang, X. Zhu, and J. Cheng, Nat. Commun. **9**(1), 1632 (2018).
[24]J. Chen, J. Xiao, D. Lisevych, A. Shakouri, and Z. Fan, Nat. Commun. **9**, 4920 (2018).
[25]Y. Zhou, M. H. Lu, L. Feng, X. Ni, Y. F. Chen, Y. Y. Zhu, S. N. Zhu, and N. B. Ming, Phys. Rev. Lett. **104**, 164301 (2010).
[26]R. A. Jahdali and Y. Wu, Appl. Phys. Lett. **108**, 031902 (2016).
[27]X. Y. Yang, H. T. Liu, and P. Lalanne, Phys. Rev. Lett. **102**, 153903 (2009).
[28]A. Grbic and R. Merlin, IEEE Trans. Antennas Propag. **56**, 3159 (2008).
[29]A. Grbic, L. Jiang, and R. Merlin, Science **320**, 511 (2008).
[30]J. Chen, J. Rao, D. Lisevych, and Z. Fan, Appl. Phys. Lett. **114**, 104101 (2019).